Atmos. Meas. Tech., 8, 5023–5038, 2015
www.atmos-meas-tech.net/8/5023/2015/
doi:10.5194/amt-8-5023-2015

Atmospheric Measurement Techniques
Open Access
EGU

Accurate mobile remote sensing of XCO_2 and XCH_4 latitudinal transects from aboard a research vessel

F. Klappenbach[1], M. Bertleff[1], J. Kostinek[1], F. Hase[1], T. Blumenstock[1], A. Agusti-Panareda[2], M. Razinger[2], and A. Butz[1]

[1]IMK-ASF, Karlsruhe Institute of Technology (KIT), Hermann-von-Helmholtz-Platz 1, 76344 Eggenstein-Leopoldshafen, Germany
[2]The European Centre for Medium-Range Weather Forecasts (ECMWF), Shinfield Park, Reading, RG2 9AX, UK

Correspondence to: F. Klappenbach (friedrich.klappenbach@kit.edu)

Received: 2 June 2015 – Published in Atmos. Meas. Tech. Discuss.: 20 July 2015
Revised: 17 November 2015 – Accepted: 18 November 2015 – Published: 1 December 2015

Abstract. A portable Fourier transform spectrometer (FTS), model EM27/SUN, was deployed onboard the research vessel *Polarstern* to measure the column-average dry air mole fractions of carbon dioxide (XCO_2) and methane (XCH_4) by means of direct sunlight absorption spectrometry. We report on technical developments as well as data calibration and reduction measures required to achieve the targeted accuracy of fractions of a percent in retrieved XCO_2 and XCH_4 while operating the instrument under field conditions onboard the moving platform during a 6-week cruise on the Atlantic from Cape Town (South Africa, 34° S, 18° E; 5 March 2014) to Bremerhaven (Germany, 54° N, 19° E; 14 April 2014). We demonstrate that our solar tracker typically achieved a tracking precision of better than 0.05° toward the center of the sun throughout the ship cruise which facilitates accurate XCO_2 and XCH_4 retrievals even under harsh ambient wind conditions. We define several quality filters that screen spectra, e.g., when the field of view was partially obstructed by ship structures or when the lines-of-sight crossed the ship exhaust plume. The measurements in clean oceanic air, can be used to characterize a spurious air-mass dependency. After the campaign, deployment of the spectrometer alongside the TCCON (Total Carbon Column Observing Network) instrument at Karlsruhe, Germany, allowed for determining a calibration factor that makes the entire campaign record traceable to World Meteorological Organization (WMO) standards. Comparisons to observations of the GOSAT satellite and concentration fields modeled by the European Centre for Medium-Range Weather Forecasts (ECMWF) Copernicus Atmosphere Monitoring Service (CAMS) demonstrate that the observational setup is well suited to provide validation opportunities above the ocean and along interhemispheric transects.

1 Introduction

Carbon dioxide (CO_2) and methane (CH_4) are the most important anthropogenic greenhouse gases (Stocker et al., 2013). To understand their emission and uptake processes at the Earth's surface, inverse modeling approaches exploit the observed variability of the atmospheric concentration fields (e.g., Peters et al., 2007; Chevallier et al., 2010; Peylin et al., 2013). Estimating surface fluxes of CO_2 and CH_4 in particular requires accurate as well as spatially and temporally dense observations of the atmospheric abundances. Such observations have been delivered for decades by ground-based in situ monitoring stations (e.g., Masarie et al., 2014), though their coverage in remote regions is sparse. Remote sensing of column-average CO_2 (XCO_2) and CH_4 (XCH_4) from satellites is an emerging technique that promises improved coverage and data density but faces challenging accuracy requirements on the order of fractions of a percent (e.g., Chevallier et al., 2007; Bergamaschi et al., 2009). Therefore, XCO_2 and XCH_4 soundings recorded by satellites such as Scanning Imaging Absorption Spectrometer for Atmospheric CHartographY (SCIAMACHY), Greenhouse Gases Observing Satellite (GOSAT) (Burrows et al., 1995; Bovensmann et al., 1999), or the recently launched Orbiting Carbon

Observatory-2 (OCO-2) require thorough validation through ground-based measurements.

To this end, the Total Carbon Column Observing Network (TCCON) has been established. Currently operating more than 20 ground-based high-resolution lab Fourier transform spectrometers (FTS) at stations worldwide (Wunch et al., 2011; TCCON-Wiki, 2015). These ground-based FTS collect solar absorption spectra in direct-sun view allowing for accurate knowledge of the light path through the atmosphere and thereby, avoiding one of the largest sources of error for satellite remote sensing of XCO_2 and XCH_4 (Rayner and O'Brien, 2001). The typical accuracy of TCCON spectrometers is reported better than 0.8 ppm (parts per million) for XCO_2 and 7 ppb (parts per billion) for XCH_4 (Wunch et al., 2010). The TCCON FTS operate at high spectral resolution and therefore, require stationary containers that can house the rather bulky and delicate instruments. Developments are underway to prove performance of smaller and more robust remote sensing instruments that can be easily deployed in remote regions, in larger numbers, and on mobile platforms (Kobayashi et al., 2010; Krings et al., 2011; Kawasaki et al., 2012; Petri et al., 2012; Gisi et al., 2012; Frey et al., 2015).

Here, we demonstrate performance of such a small and robust spectrometer for accurate observations of XCO_2 and XCH_4 on a mobile platform. We deployed a Bruker™ EM27/SUN FTS aboard the German research vessel (RV) *Polarstern* traveling from South Africa to Germany during a 5-week cruise in March/April 2014.

The EM27/SUN FTS is a table-top, portable instrument operating at medium spectral resolution of 0.5 cm^{-1}. Performance of the EM27/SUN FTS in stationary configuration has been proven for XCO_2 by Gisi et al. (2012) using measurements alongside the TCCON instrument at Karlsruhe, Germany. Previously, Notholt et al. (1995) and Warneke et al. (2005) have shown that RV *Polarstern* is an excellent carrier to investigate hemispheric gradients of a large variety of atmospheric constituents including the man-made greenhouse gases. Instrumentation, however, is challenged by harsh ambient conditions. In particular, the moving platform poses a challenge for direct solar absorption spectroscopy since the solar intensity has to be fed precisely into the spectrometer's entrance aperture, irrespective of the movements of the platform. In the view of satellite validation, shipborne measurements are particularly interesting since currently there are only a few island observatories (e.g., Geibel et al., 2010; Schneider et al., 2012) that allow for validating XCO_2 and XCH_4 derived from glint-mode satellite operations over the oceans.

Figure 1 illustrates the track of RV *Polarstern*, started out at Cape Town, South Africa (34° S, 18° E) on 5 March 2014, and entered port at Bremerhaven, Germany, (54° N, 19° E) on 14 April 2014. During the cruise the EM27/SUN spectrometer operated whenever cloud conditions permitted direct-sun view on 31 out of 40 days, in total collecting 5738 spectra for which XCO_2 and XCH_4 could be derived. Beside recording solar absorption spectra, our housekeeping infrastructures monitored ambient pressure and temperature. Further, RV *Polarstern* is equipped with a meteorological station. In addition to the EM27/SUN, we operated a custom-built grating spectrometer. Design and performance of the latter will be reported in a forthcoming study.

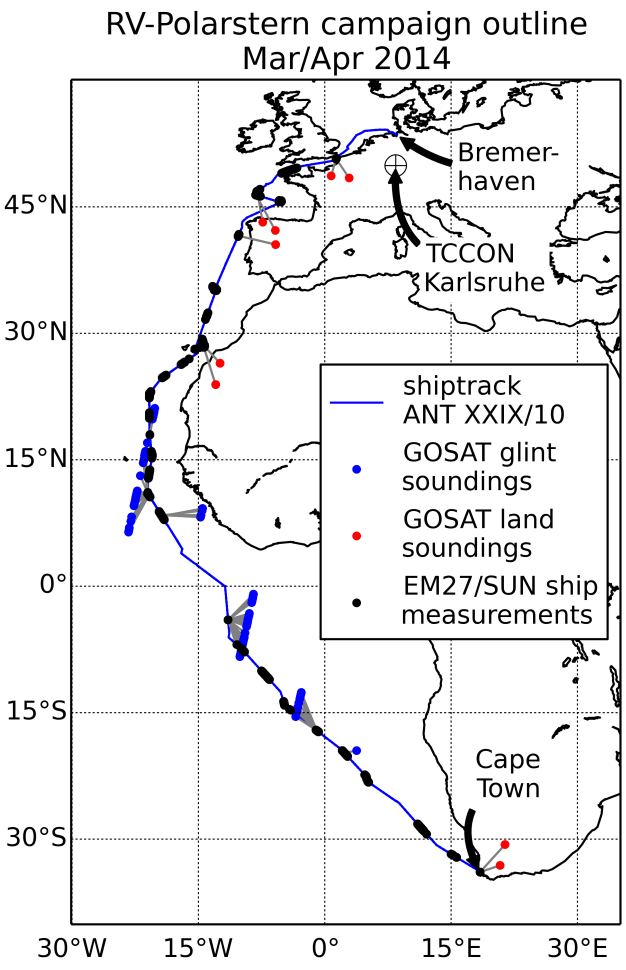

Figure 1. The ship track of the ANT XXIX/10 RV *Polarstern* cruise (blue line). Valid data are marked black. GOSAT-soundings that coincide with ship-based measurements within ±4 h and 5° (lat, lon) are marked in blue (ocean) and red (land) and interconnected (gray lines).

Here, we first outline the instrument setup (Sect. 2) in particular focusing on a custom-built sun-tracker attached to the sun-viewing spectrometer. The sun-tracker must be able to compensate both the relatively slow motion of the solar disk across the sky and the (occasionally) fast movements of the platform. Then, we detail data reduction measures to guarantee the high accuracy and consistency of the XCO_2 and XCH_4 soundings throughout the ship cruise (Sect. 3). Finally, we illustrate the usefulness of the derived greenhouse gas concentrations for validation soundings from GOSAT

and for evaluating the hemispheric concentration gradients in a global model (Sect. 4). Section 5 concludes the study.

2 Instrumentation

The key instrumentation was an EM27/SUN FTS (Sect. 2.2) available for purchase at Bruker™ Optics together with a custom-built solar tracker (Sect. 2.1).

2.1 Custom-built solar tracking system

The solar tracker used was based on the "Cam-tracker" setup initially designed for stationary platforms by Gisi et al. (2011). Here, it was modified for mobile applications and its performance could be demonstrated through its operation on RV *Polarstern*: the system consists of two mirrors that rotate along an azimuth and elevation axis driven by two stepper motors, and it is able to point toward every point on the sky hemisphere above the instrument. A camera observes the solar image centered about the entrance aperture of the spectrometer. An image analysis software fits circles to the solar image and the aperture. The mismatch between the circle centers drives a PID (proportional-integral-differential) control unit which adjusts the mirrors to finally recenter the solar image. On stationary platforms, PID (proportional-integrational-differential) control cycles exceeding a second are acceptable given that the solar disk moves slowly ($< 0.005^\circ\,s^{-1}$) across the sky. Under such conditions, Gisi et al. (2011) showed that tracking errors are typically less than 0.003° which was well below the targeted tracking accuracy of 0.05° needed to keep pointing-induced XCO_2 errors below 0.1 ppm.

Adapting the solar tracking system to mobile applications posed the following two major challenges.

- At start-up or after interruptions of the tracking operations, the solar tracker needs to find the solar disk without knowledge of the observatory's orientation. For stationary operations the attitude of the observatory is typically given at start-up (and left unchanged) and astronomical calculations provide the initial relative position of the sun.
- The PID control cycle needs to cope with the potentially fast motion of the platform in addition to the slow motion of the solar disk.

Basically, the used tracking procedure can be split into two parts that tackled the required adaptations: the coarse and the fine-tracking mode. The latter is a refinement of the concept proposed by Gisi et al. (2011). Both required additional or exchange of hardware.

The coarse-tracking mode relied on a 185° fish eye-lens (Lensation, BFM2320) that was mounted on a CMOS digital camera (VR-magic, model C-9+ PRO BW CMOS, 1288 × 1032 pixel) that observed the sky hemisphere above the instrument. The brightest spot on the camera image gave the approximate position of the solar disk. A lookup table that was generated through lamp calibration in our laboratory translated image positions into azimuth and elevation angles of the tracking mirrors. The angular resolution of the coarse tracking is approximately $0.15^\circ\,\text{pixel}^{-1}$ and is strongly variable within the field of view. Thus, it is not accurate enough to perform the entire tracking process with the desired accuracy of 0.05°. However, the coarse-tracking ensures that the solar disc of about 0.53° diameter can be located within the field of view (FOV) of the fine-tracking camera in the range of 10–15°.

Table 1. Leading contributions to the duration of fine-tracking control cycles of the solar tracker (average values retrieved from housekeeping data logged during the measurement campaign aboard RV *Polarstern*).

Task	Duration ms
Image acquisition	≈ 10
Image processing	< 3
Motor position request	5–10
Update motor speed	5–10
Overall average	≈ 22

Once the solar image was within the FOV of the fine-tracking camera (VR-magic, model C-9+ PRO BW CMOS, 1288 × 1032 pixel, $f = 50$ mm), coarse tracking went idle and fine-tracking mode took over and centered the solar image on the aperture of the spectrometer through a circle fitting routine. In order to enhance the tracking velocity for a moving platform, it was essential to update the motor control parameters (position, speed, or acceleration) as frequently as possible. To minimize the time lost during communication between the fine-tracking camera and the control unit (embedded PC system, ARK-2150 by Advantech), the camera only transmitted a region of interest of approximately 200 pixel × 200 pixel out of the full camera frame of 1288 pixel × 1032 pixel via USB. Additionally each motor was connected via its own RS485 connection to the control unit to enable simultaneous send and receive to/from both motors. Based on this hardware setup, our custom-built image acquisition, processing, PID and motor control software achieved control cycle durations on the order of 20–30 ms corresponding to an update frequency of 33–50 Hz. Table 1 summarizes individual contributions.

We evaluate the onboard performance of the solar tracker by examining the deviations between the center of the solar image and the targeted center of the spectrometer aperture. The deviations were logged during the entire campaign on board RV *Polarstern*. While such an assessment provides an estimate of the tracking precision, it does not allow for quantifying systematic tracking errors, e.g., due to a misalignment of the actual and the assumed center of the spectrometer aperture. A misalignment of the latter kind would lead to a sys-

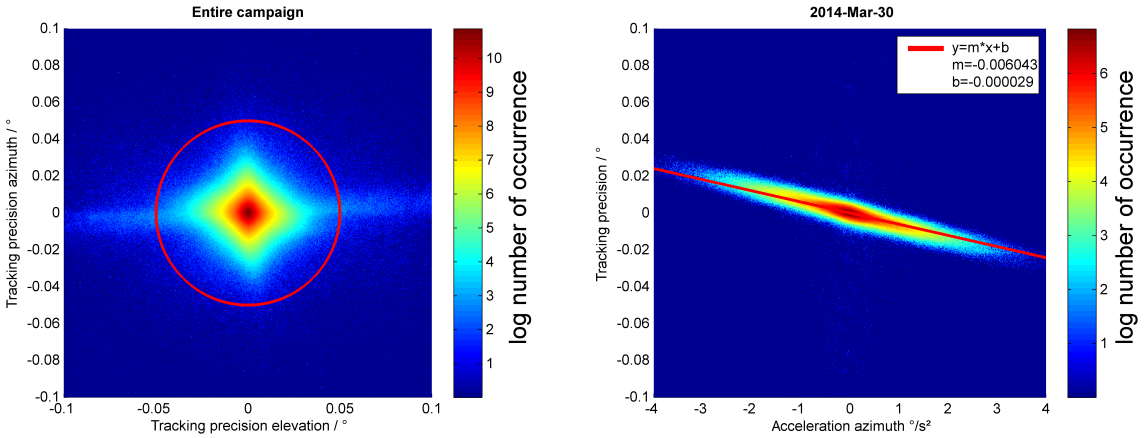

Figure 2. Both figures show occurrence of tracking errors in logarithmic color code. The left figure counts azimuth and elevation tracking errors for the entire campaign record. The red circle defines the desired 0.05° tracking precision. 98.7 % of the data points are within the circle. The right figure shows azimuth tracking precision vs. angular azimuthal acceleration for a representative day with significant angular accelerations due to a rougher sea than other days.

tematic pointing offset, i.e., the solar tracker does not point exactly to the center of the sun but slightly to the limb. However, the fine-tracking camera and aperture were carefully aligned in the lab to avoid such systematic errors.

Figure 2 (left) shows the logarithmic occurrence count of tracking deviations in azimuth and elevation directions. The desired tracking accuracy of 0.05° is red encircled. 98.7 % of the entire campaign data are within this tracking error regime. The record includes all kinds of interruptions such as shadowing by the ship's infrastructure or cloudy conditions. The tracking accuracy of the entire data accounts for 0.0076° (1σ), which means, that 68.3 % of all data points feature an accuracy of this value or better. The origin of the star-shape pattern remains unclear.

Figure 2 (right) shows the dependency of the tracking precision on the angular acceleration for an illustrative day of the ship cruise. Because the PID parameters were changed along the entire cruise, we focus on that representative day. To simplify the evaluation, we analyze just the azimuth component. The azimuth component is physically the most inert part of the system and serves as a conservative estimate. The elevation component, however, shows very similar behavior. Generally, the larger the accelerations required to compensate ship movements, the poorer the tracking precision. The linear dependency of tracking precision on angular acceleration can be used to derive a maximum acceleration up to which our solar tracking performs within the required limits: as long as the angular acceleration did not exceed approximately 6.5° s^{-2}, the tracking precision complied with the 0.05° requirement.

2.2 Fourier transform spectrometer EM27/SUN

The Bruker™ EM27/SUN FTS is a table-top Fourier transform spectrometer of approximately 25 kg weight. It was designed in the framework of a cooperation between KIT and Bruker™ for stationary XCO_2 and XCH_4 measurements (Gisi et al., 2012). Here, we give a brief overview of the most important features.

The EM27/SUN is constructed as a RockSolid™ pendulum interferometer with two cube corner mirrors and a CaF_2 beam splitter. The optical path difference of 1.8 cm corresponds to a spectral resolution of 0.5 cm^{-1}. A 127 mm parabolic mirror together with the 0.6 mm aperture defines an semi-FOV of 2.36 mrad. With the solar disc as light source, this FOV corresponds to approximately 51.0 % of the solar diameter. The InGaAs non-cooled detector (HAMAMATSU™ G12181-010K) with a sensitive area of approximately 0.8 mm^2, has a spectral response from 5000 to 11 000 cm^{-1}. Typical exposure times are approximately 58 s for 10 double sided interferograms, recorded in DC-mode. Differences to the prototype device used by Gisi et al. (2012) are a slightly different focal length of 127 mm instead of 101.6 mm and a detector with a spectral coverage of 5000 to 11 000 cm^{-1} instead of 6000 to 9000 cm^{-1}. The latter adjustment was necessary to cover the spectral range of CH_4 absorption. Further, a bandpass filter (Thorlabs FB1650-12, center wavenumber: 6061 cm^{-1}, FWHM (full width at half maximum): 44.0 cm^{-1}) has been mounted in front of the internal calibration lamp in order to characterize the ghost-to-parent ratio as described in Dohe et al. (2013) or Messerschmidt et al. (2010).

Gisi et al. (2012) showed, that this instrument is highly stable against thermal influences in particular as demonstrated by observations in summer and winter in Karlsruhe. Furthermore moderate mechanical stress due to deployment and dismounting do not harm the accuracy of the instrument. This makes the instrument in particular suitable for campaign purposes.

Table 2. List of key retrieval parameters. The line lists are altered from the original HITRAN line lists where "mod" indicates a modification suggested by Lamouroux et al. (2010) to take line mixing effects into account. Likewise "TCCON" indicates a modification suggested by Wunch et al. (2011).

	CO_2	CH_4	O_2	H_2O
Spectral window cm^{-1}	6173–6390	5897–6145	7765–8005	8353.4–8463.1
Line list	HITRAN08 (mod)	HITRAN08	HITRAN08 (TCCON)	HITRAN09 (TCCON)
Disturbing gas	H_2O, CH_4	H_2O, CO_2	H_2O	–
Continuum points	40	20	25	5
SZA dependency ($\Theta = 80°$)	$\approx 0.6\,\%$	$\approx 0.4\,\%$	none	not assessed
A priori profile	CAMS	CAMS	static	CAMS

3 Data reduction and evaluation

The following section guides through the data evaluation process. Section 3.1 describes the spectral retrieval of absorber total columns from the recorded solar absorption spectra. Various quality filters (Sect. 3.2) and corrections (Sect. 3.3) guarantee that quality of the estimated XCO_2 and XCH_4 is consistently high throughout the ship cruise.

3.1 Spectral retrieval

We used the software package PROFFIT v.9.6 (Hase et al., 2004) for the spectral retrieval of absorber total columns. In principle, PROFFIT is capable of retrieving vertical profile information from high spectral resolution measurements of the atmospheric transmittance in direct-sun view (García et al., 2012). The medium resolution of $0.5\,cm^{-1}$ of the EM27 FTS, however, is insufficient to extract profile information from the pressure and temperature dependent absorption line shapes. Therefore, here, we chose a configuration that retrieved a scaling parameter for the a priori absorber profiles. In particular the number of degrees of freedom (DOF) was chosen to be one (DOF = 1).

The absorber total columns to be retrieved were the ones of the targeted species CO_2 and CH_4, and the ones of the ancillary species molecular oxygen (O_2) and water vapor (H_2O). The latter is an interfering species. O_2 was used to calculate the dry air mole fraction X_{gas} of the desired target gas via

$$X_{gas} = 0.209420 \cdot \frac{C_{gas}}{C_{O_2}} \quad (1)$$

where C_{gas} is the gas total column in units $molec\,m^{-2}$. Referencing the targeted gas abundance to the known O_2 abundance is a common approach to cancel out instrument and retrieval related errors common to the retrievals of O_2 and the target species.

The a priori profiles of CO_2 and CH_4 are taken from the CAMS global cyclic 1-day forecasts which are based on the ECMWF Integrated Forecasting System (IFS) as documented by (Agustí-Panareda et al., 2014; Massart et al., 2014). The H_2O profiles are from the IFS 1-day forecasts extracted from the same model simulation as CO_2 and CH_4.

We interpolated all profiles temporally and spatially on the model grid ($0.5° \times 0.5° \times 3$ hourly) in order to avoid discontinuities. The top level of the CAMS data (0.1 hpa $\approx$ 65 km height) was extrapolated upon $\approx$ 120 km height in order to fit the layers of the meteorological profiles described below. Meteorological parameters such as pressure and temperature vertical profiles were based on the monthly latitudinal mean profiles provided by CIRA-86[1] (Fleming et al., 1988) that reaches up to 120 km height in 77 levels. If available, these meteorological profiles were supplemented by the daily noon-time radiosonde measurements from aboard RV *Polarstern* that reached altitudes up to 30 km height (König-Langlo, 2014). If no radiosonde data were available, the data from the global model reanalysis from the National Centers for Environmental Prediction (NCEP) (Kalnay et al., 1996) was used to supplement the initial profile up to approximately 30 km height. The NCEP data were downloaded via the Goddard auto mailer system (Schoeberl et al., 2014). This combined profile was interpolated on a 49 layer grid from measurement height up to 120 km.

The a priori O_2 profile a priori was a generic static profile, that represented a typical situation.

We used the High Resolution Transmission (HITRAN) database (Rothman et al., 2009) from 2008 to calculate the atmospheric gas absorption lines. While as we left the line list for CH_4 unchanged, we modified the line lists of CO_2 as suggested by Lamouroux et al. (2010) to take line-mixing effects into account. The line list for O_2 was modified according to TCCON recommendations. Finally, the H_2O line list was based on HITRAN updates from 2009.

Table 2 gives an overview of the most important retrieval parameters among the various spectral windows.

[1]CIRA stands for "COSPAR International Reference Atmosphere", whereas COSPAR stands for "Committee on Space Research".

The instrumental line shape (ILS) of the instrument was determined analyzing water vapor absorption lines along a light path through ambient air in our laboratory. We collimated a 50 W light bulb and positioned at ~ 4.0 m distance to the spectrometer. A data logger (MRC, MHB-382SD) provided temperature and pressure readings and allowed to calculate the appropriate absorption line shapes. Parameters defining the ILS are retrieved together with the ambient H_2O abundance from absorption spectra in the spectral range at 7000–7400 cm^{-1} using the LINEFIT software package version 14 (Hase et al., 1999). We found ILS parameters 0.99594 for the modulation efficiency and 2.83×10^{-3} for the phase error in the post campaign retrieval. As long as no instrumental changes (e.g., accidental or intentional changes in the optical alignment) are undertaken, the inferred ILS parameters were shown to be constant over month-long timescales (Gisi et al., 2012; Frey et al., 2015).

We performed the pre-processing with the Python routine "Calpy_mobile" program developed at KIT. This routine requests and downloads the meteorological profile data at the Goddard auto-mailer system and generates the input profiles with the radiosonde data. Additionally it performs the DC correction (Keppel-Aleks et al., 2007a) (see Sect. 3.3) on the interferogram, the Fourier transformation and finally exports it into a binary input format for PROFFIT.

3.2 Quality filters

We operated the spectrometer semi-automatically from morning to afternoon on deck of the RV *Polarstern* whenever outside weather conditions were not too harsh. Therefore, spectra were recorded also under unfavorable conditions, e.g., when the sun was partially obscured by ship structures or when lines-of-sight crossed the exhaust plume (EP) of the ship. To exclude such measurements from the scientific data set, we applied three quality filters: the DC filter screened strong intensity fluctuations. The O_2 filter gave an estimate on the retrieval quality with the ground pressure as reference. Finally the EP filter (exhaust plume) removed measurements, where the instrument's line of sight passed the ships exhaust plume.

The DC filter was designed to sort out intensity fluctuations during the measurement. These fluctuations can for example be introduced by variable cirrus clouds or by the ship's structures obscuring the line of sight. We operated the EM27/SUN FTS in the DC mode, i.e., the spectrometer recorded the full interferogram including its smoothly varying DC part. Strong fluctuations in the DC part are indicative for varying source brightness. Affected measurements can be corrected with the low pass filtered interferogram I_{lp} (Keppel-Aleks et al., 2007b). The implementation of the low pass was a running mean on the interferogram over 61 sampling points with 5 iterations.

However, this DC correction did not remove the entire DC effect, and especially strong variations still appear to influence the retrieval result. Based on the DC correction, we defined a filter criterion DC to sort out affected measurements:

$$\mathrm{DC} = \frac{|I_{lp}|_{max} - |I_{lp}|_{min}}{|I_{lp}|_{max}}. \quad (2)$$

The higher the value of the DC criterion, the stronger the effect on the retrieved trace gas. Effects of the DC filter are examined in Figs. 3 and 4 and discussed together with the next filter. Here, we choose a filter threshold DC < 0.05 that discards 23.2 % of the recorded spectra.

The O_2 filter was based on the comparison between surface pressure calculated from the retrieved O_2 column and the in situ measured surface pressure (König-Langlo, 2014) as suggested by Wunch et al. (2011). Deviations indicate a false measurement since the O_2 concentration in the atmosphere can be assumed constant. We took a scaling factor of 0.9705 into account for calibrating the spectroscopically retrieved surface pressure p_{retr} to the in situ measurements $p_{in\ situ}$ (Wunch et al., 2011), the ratio

$$R_{psf} = \frac{0.9705 \times p_{O_2\,dry} + p_{H_2O}}{p_{in\ situ}} \quad (3)$$

scatters around unity. Here, we screened spectra whenever R_{psf} deviated by more than 0.3 % from unity removing 6.3 % of the DC-filtered spectra. We determined the filter thresholds for both the DC and O_2 filters by the definition of a quality criterion Q for the retrieved XCO_2: we selected a subset of representative days from 22 to 25 March 2014. First, we removed diurnal variations from the record by fitting a 3rd order polynomial for each day and subtracted the polynomial from the retrieved XCO_2. The standard deviation of the

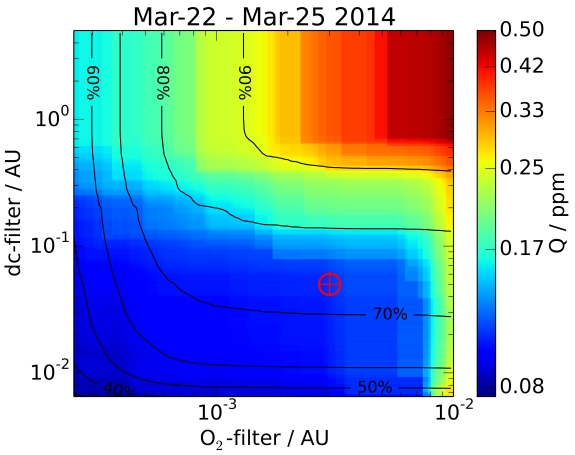

Figure 3. Effect of filter threshold for the O_2 filter (abscissa) and the DC filter (ordinate) on the standard deviation of retrieved XCO_2 (color coded in logarithmic scale). Standard deviation of XCO_2 is calculated for 4 sample days after subtracting a 3rd order polynomial that accounts for diurnal and day-to-day variability. The data yield is overlayed as solid black contours. The finally chosen filter thresholds (5 % for the DC filter and 0.3 % for the O_2 filter) are marked with the red marker.

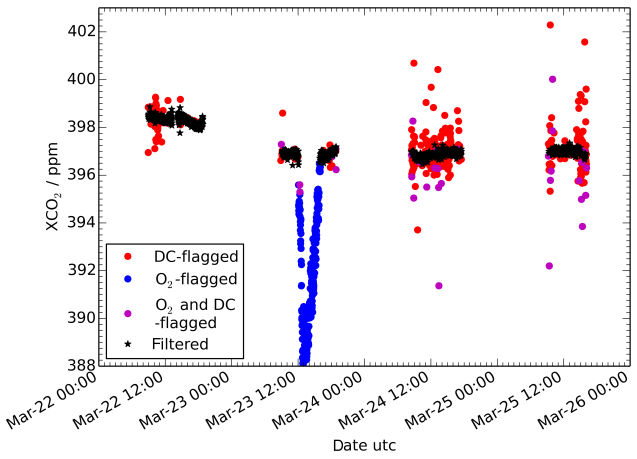

Figure 4. Effect of the DC filter and the O_2 filter on the retrieved XCO_2 for 4 sample days during the campaign. The outlier on 23 March that is caught by the O_2 filter originates from a malfunction of the sun tracker that caused unstable pointing. The days after were affected by small but opaque clouds that disturbed some measurements which are caught by the DC filter.

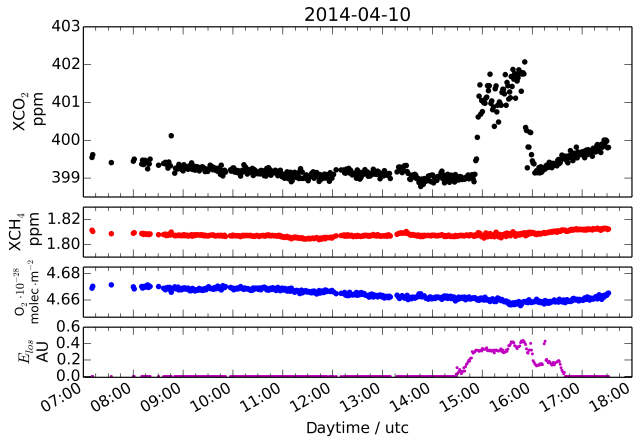

Figure 5. XCO_2 (top) record for a representative day after applying the DC and O_2 quality filters. The XCH_4 (upper middle, red) and O_2 (lower middle, blue) retrievals indicate no enhancements. In contrast, the XCO_2 enhancement of more than 2 ppm between 3 and 5 p.m. can be related to the lines of sight crossing the ship's exhaust plume. The calculated enhancement E_{los} (bottom) drives the EP filter with a rejection threshold set at 0.001.

residual XCO_2 time series now defines our quality criterion Q in units of ppm.

Figure 3 illustrates how the DC filter and the O_2 filter affects the quality criterion $Q_{\mathrm{XCO_2}}$. In general the stricter the filter thresholds the better the precision but the fewer data passing the quality filters. Figure 4 shows the XCO_2 measurements for these 4 representative days and the effect of the DC and O_2 filters with the selected thresholds. The overlap of the two filters is very little, showing that they filter for independent effects.

Under the assumption that the 3rd order polynomial removed all geophysical variability due to local surface fluxes and advective transport, this quality criterion provides a precision estimate for the EM27/SUN amounting to $Q_{\mathrm{XCO_2}} = 0.11$ ppm for XCO_2. Following an analogous procedure for XCH_4 yields $Q_{\mathrm{XCH_4}} = 0.61$ ppb.

The third filter is the exhaust-plume filter (EP filter). The ship's funnel was located at a few tens of meters distance to the spectrometer setup and rose to approximately 12 m above deck. If the line of sight passed through the exhaust plume, enhancements in the observed XCO_2 were to be expected. In order to screen such observations, we calculated the enhancement pattern in the XCO_2 time series from our line of sight (los), the prevailing wind conditions, and the ship's exhaust.

An estimated exhaust flux E_s fed a simple plume model that calculated the XCO_2 enhancement E_{los} and took into account the relative wind speed and direction between the ship-based spectrometer and the plume. We relied hereby on the plume diffusion model from Bovensmann et al. (2010). Defining the x coordinate as downwind direction and the y coordinate as the crosswind direction, the enhancement E_{los} along the line of sight could be calculated via

$$E_{\mathrm{los}} = \int^{\mathrm{los}} \frac{E_s}{v_{\mathrm{rel}}} \frac{1}{\sqrt{2\pi}\cdot\sigma_y(x)} \cdot \exp\left(-\frac{1}{2}\frac{y^2}{\sigma_y(x)^2}\right) \mathrm{d}x\,\mathrm{d}y, \quad (4)$$

where v_{rel} is the relative wind velocity between ship and plume, and the parameter $\sigma_y(x) = 0.104 \cdot x^{0.894}$ dilutes the plume in crosswind direction (y). Thereby, we assume a class C for the atmospheric stability (Bovensmann et al., 2010). Here the exhaust flux $E_s := 1$ is given in arbitrary units (AU). Relative wind velocities v_{rel} and directions were taken from the records of the onboard meteorological station. The line of sight from instrument position up to 30 m was projected into the downwind (x) and crosswind (y) direction and then, E_{los} was calculated by numerically integrating Eq. (4). Figure 5 shows a day where according to the lab book the line of sight passed the exhaust plume as confirmed by the record of relative wind velocities and directions. Measured O_2 columns and XCH_4 were not affected by the ship's exhaust, XCO_2, however, were found enhanced by up to 2 ppm. Our model yielded an enhancement E_{los} that was similar in temporal pattern to the observed XCO_2 enhancement that confirmed the overall applicability of our approach.

The EP filter threshold was set such that whenever E_{los} was larger than 0.001 the spectrum was flagged contaminated. 11.1 % of the spectra were discarded by the EP filter. Additionally, 2.8 % of the spectra were rejected due to contamination by the exhaust plume after inspection by eye.

In total, the three filters (DC, O_2, and EP) described above screened about 38.2 % of the recorded spectra.

3.3 Corrections

Two major corrections were necessary to make the XCO_2 and XCH_4 records consistently accurate along the ship cruise: a spurious dependency of the retrieved target gas abundances on solar zenith angle needed to be corrected, and an overall calibration factor needed to be found to make the spectroscopic measurements consistent with the WMO (World Meteorological Organization) calibration scale.

We could reproduce a well known (e.g., Deutscher et al., 2010; Wunch et al., 2011), spurious dependency of XCO_2 and XCH_4 retrieved from TCCON measurements on slant air-mass A, defined as $A = 1/\cos(\theta)$ with solar zenith angle θ, with our campaign data. With increasing air mass, the XCO_2 and the XCH_4 retrievals tend to be lower. The source of this effect remains unclear, although uncertainties of spectroscopic line broadening parameters and shortcomings of the Voigt line shape model are likely candidates. Wunch et al. (2011) suggested an empirical correction based on a diurnal effect combined with a θ-dependent term. Figure 6 shows that also our XCO_2 and XCH_4 retrievals clearly correlate with SZA. Given that the retrieved surface pressure derived from retrieved O_2 columns did not show such dependency, it must have been driven by the CO_2 and CH_4 column retrievals. To correct for this artifact, we fitted a correction polynomial $c_{\mathrm{SZA,\,gas}}$ for the gases CO_2 and CH_4 according to

$$c_{\mathrm{SZA,\,gas}}(\theta) = a \cdot |\theta|^3 + b \cdot |\theta| + c, \tag{5}$$

where a, b, and c are free fit parameters. Thereby, the correction was by definition chosen to vanish at $\theta = 45°$ as suggested by Wunch et al. (2011) with referencing the measurement to $\theta = \pm 45°$ for forenoon and afternoon separately. The corrected XCO_2 and XCH_4 records are then calculated through

$$X_{\mathrm{SZA,\,gas}} = \frac{X_{\mathrm{gas}}(\theta)}{c_{\mathrm{SZA,gas}}(\theta)}. \tag{6}$$

Figure 6 shows the retrieved correction parameters. For the extreme case of $\theta = 80°$ relative to $\theta = 0°$, the correction amounts to $\approx 0.4\,\%$ for XCO_2 and $\approx 0.3\,\%$ for XCH_4. A key assumption for this correction is that the measurements took place far away from localized sources and sinks of CO_2 and CH_4. So, no diurnal concentration cycles were to be expected that correlate with the assumed spurious air-mass dependence. Generally, this assumption appeared to be true for our ship-borne measurements above the Atlantic. Meteorological transport can cause advection of diurnal concentration variability from the larger source/sink region. Over the course of the entire measurement campaign, we assume that such transport effects have a statistical pattern such that the air-mass correction is not contaminated in a systematic way.

Finally, we calibrated the entire campaign records to those of the TCCON station at Karlsruhe, Germany (Hase et al., 2015), which in turn is calibrated to WMO standards according to TCCON requirements. TCCON XCO_2 and XCH_4 were retrieved with the GGG2014 software package (Wunch et al., 2011, 2015). We operated the campaign instrument alongside the Karlsruhe TCCON instrument during 4 consecutive days in May 2014 after the ship campaign. Retrievals from the EM27/SUN measurements followed the approach outlined in Sect. 3 including the quality filters described in Sect. 3.2 and the aforementioned correction terms. Hourly means $\langle X \rangle_{\mathrm{h}}$ of the XCO_2 and XCH_4 were calculated and used to determine the calibration factor γ_{gas} according to

$$\gamma_{\mathrm{gas}} = \left\langle \frac{\langle X_{\mathrm{EM27}} \rangle_{\mathrm{h}}}{\langle X_{\mathrm{wmo}} \rangle_{\mathrm{h}}} \right\rangle, \tag{7}$$

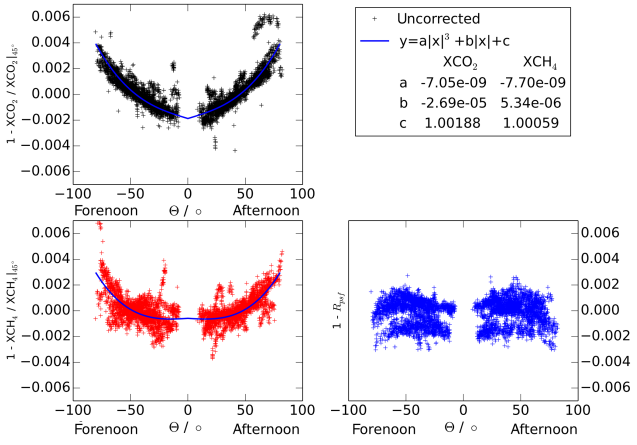

Figure 6. SZA dependency for CO_2 (upper left, referenced to XCO_2 at forenoon/afternoon SZA = 45°), CH_4 (lower left, referenced to XCH_4 at forenoon/afternoon SZA = 45°), and O_2 (lower right, surface pressure referenced O_2 retrieval R_{psf} (see. Eq. (3)) as a function of SZA θ. Solid lines show the fitted SZA correction function.

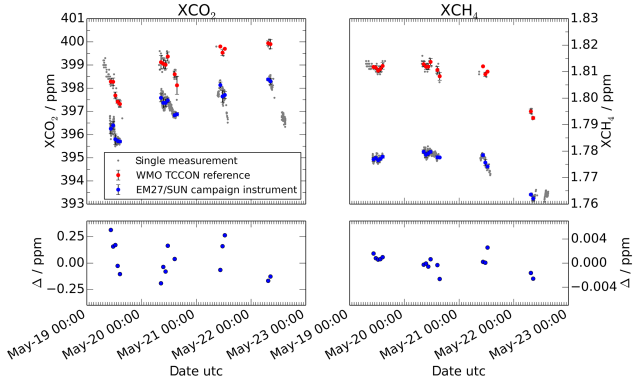

Figure 7. Post campaign measurements in Karlsruhe are used to retrieve the WMO-calibration factor for each gas. Hourly averages are taken for the TCCON reference (red) and the EM27/SUN measurements (blue). The calibration residual (lower panel) is defined as $\Delta := \langle X_{\mathrm{wmo}} \rangle_{\mathrm{h}} - \langle X_{\mathrm{gas,wmo}} \rangle_{\mathrm{h}}$.

where brackets indicate averaging over the entire data set. We then referenced the entire EM27/SUN data set to the WMO calibrated TCCON reference with the global scaling factor γ_{gas}:

$$X_{\text{gas,wmo}} = \frac{X_{\text{gas}}}{\gamma_{\text{gas}}}. \quad (8)$$

Figure 7 shows the post campaign reference measurements.

We found calibration factors $\gamma_{XCO_2} = (0.99568 \pm 0.00049)$ and $\gamma_{XCH_4} = (0.98162 \pm 0.00073)$ where the error estimate refers to the standard deviation among the calibration data set. Note that the calibration factor for O_2 (see Sect. 3.2) on the order of $\approx 2.8\,\%$ (≈ 0.972) was still present in the un-referenced data and is included in the calibration factor γ_{gas}. Note further, that this calibration was obtained with the reprocessed TCCON-Karlsruhe data set. This improvement was found to be necessary because the station Karlsruhe differs in the optical setup from other TCCON stations (M. Kiel, personal communication, 2015). The difference can be scaled by using $\gamma_{XCO_2,\text{old}}/\gamma_{XCO_2,\text{new}} = 1.00219487$ and XCH_4 by 1.00103463.

4 XCO_2 and XCH_4 over the Atlantic

Figure 8 shows the final XCO_2 and XCH_4 records measured above the Atlantic in March/April 2014 from aboard RV *Polarstern*. All corrections (see Sect. 3.3) and quality filters (see Sect. 3.2) were applied. In order to motivate the usefulness of such ship deployments for satellite and model validation, Fig. 8 additionally shows satellite soundings from the Greenhouse Gas Observing Satellite (GOSAT) and XCO_2 and XCH_4 modeled by the CAMS (Copernicus Atmosphere Monitoring Service) data assimilation and forecasting system (Agustí-Panareda et al., 2014; Massart et al., 2014). Satellite soundings were correlated to RV *Polarstern* records with a 5° latitudinal/longitudinal radius in addition with a 4 h temporal coincidence radius (see Fig. 1). Model data were temporally and spatially interpolated to the RV *Polarstern* measurements in order to avoid discontinuities.

The lower panel shows the differences of the various greenhouse gas products to the campaign record. Here averages of all EM27/SUN soundings within the coincidence criteria were subtracted from the individual satellite soundings.

For GOSAT, we discuss three different GOSAT retrieval methods, the RemoTeC-full-physics (FP) and RemoTeC-proxy (Butz et al., 2011; Guerlet et al., 2013; Schepers et al., 2012) retrieval as well as the Atmospheric CO_2 Observations from Space (ACOS) approach (O'Dell et al., 2012; Crisp et al., 2012). Even though the in-orbit operations of GOSAT have been adapted to maximize the number of ocean-glint soundings during the campaign period, the number of coincident and quality-assured retrievals amounts to a few tens of samples, that largely varied among the retrieval approaches. The main difference between the RemoTeC-FP and the RemoTeC-proxy algorithm is the way the light path through the atmosphere is estimated. While RemoTeC-FP retrieves aerosol parameters simultaneously with XCO_2 and XCH_4 and takes multiple scattering effects into account, the RemoTeC-proxy approach is restricted to XCH_4 only and uses the retrieved CO_2 column together with CarbonTracker-modeled CO_2 as a light path proxy. ACOS is, as well as RemoTeC-FP, a full-physics approach, i.e., simultaneously retrieving XCO_2 and atmospheric scattering properties. Differences between RemoTeC-FP and ACOS relate to details how aerosol and cloud scattering parameters are implemented and how the inverse problem is solved. Most importantly here, ACOS delivers many more data than RemoTeC-FP for ocean-glint soundings since RemoTeC-FP resorts to a conservative cloud and aerosol filtering scheme using the "upper edge" method (Butz et al., 2013). ACOS does not deliver XCH_4. For the comparison with all the GOSAT products the smoothing effect of the averaging kernel matrix is neglected. Compared to systematic errors introduced by temporal and spatial distance, we consider these effects to be negligible.

CAMS provides global operational analysis and forecast of CO_2 and CH_4 in near real time. Here we have used a forecast without any data assimilation with a horizontal resolution of around 80 km and 60 vertical levels from surface to 0.1 hPa. The atmospheric CO_2 and CH_4 mixing ratio fields modeled by CAMS rely on the ECMWF IFS model[2]. The IFS has a simple carbon module (Boussetta et al., 2013) to model the CO_2 uptake and release from vegetation. The CO_2 biogenic fluxes from vegetation are adjusted to correct for large-scale biases by using a climatology of optimized CO_2 fluxes (Agusti-Panareda et al., 2015, ECMWF Tech Memo 2015). The CH_4 fluxes and other CO_2 fluxes are prescribed by inventories and seasonally varying climatologies, including the chemical sinks for CH_4 in the troposphere and stratosphere. A more detailed description of the CO_2 and CH_4 forecast configuration can be found in Agustí-Panareda et al. (2014) for CO_2 and in Massart et al. (2014) for CH_4. The plotted data stem from the model simulation, where the meteorology is re-initialized daily using ECMWF meteorological analyses but CO_2 and CH_4 are free running, i.e., no assimilation of CO_2 and CH_4 observations is performed.

The EM27/SUN XCO_2 measurements from aboard RV *Polarstern*, Fig. 8 (left), show a north–south (N–S) gradient of up to 6.8 ppm between $\sim 45°$ N and $\sim 30°$ S at the end of the Northern Hemisphere dormant season. This is largely expected from previous assessments (e.g., Denning et al., 1995). Beside the N–S gradient, diurnal and day-to-day variations on the order of 1 ppm are found most likely originating from transport of far-away source/sink signals. Note that the

[2]https://software.ecmwf.int/wiki/display/IFS/Official+IFS+Documentation

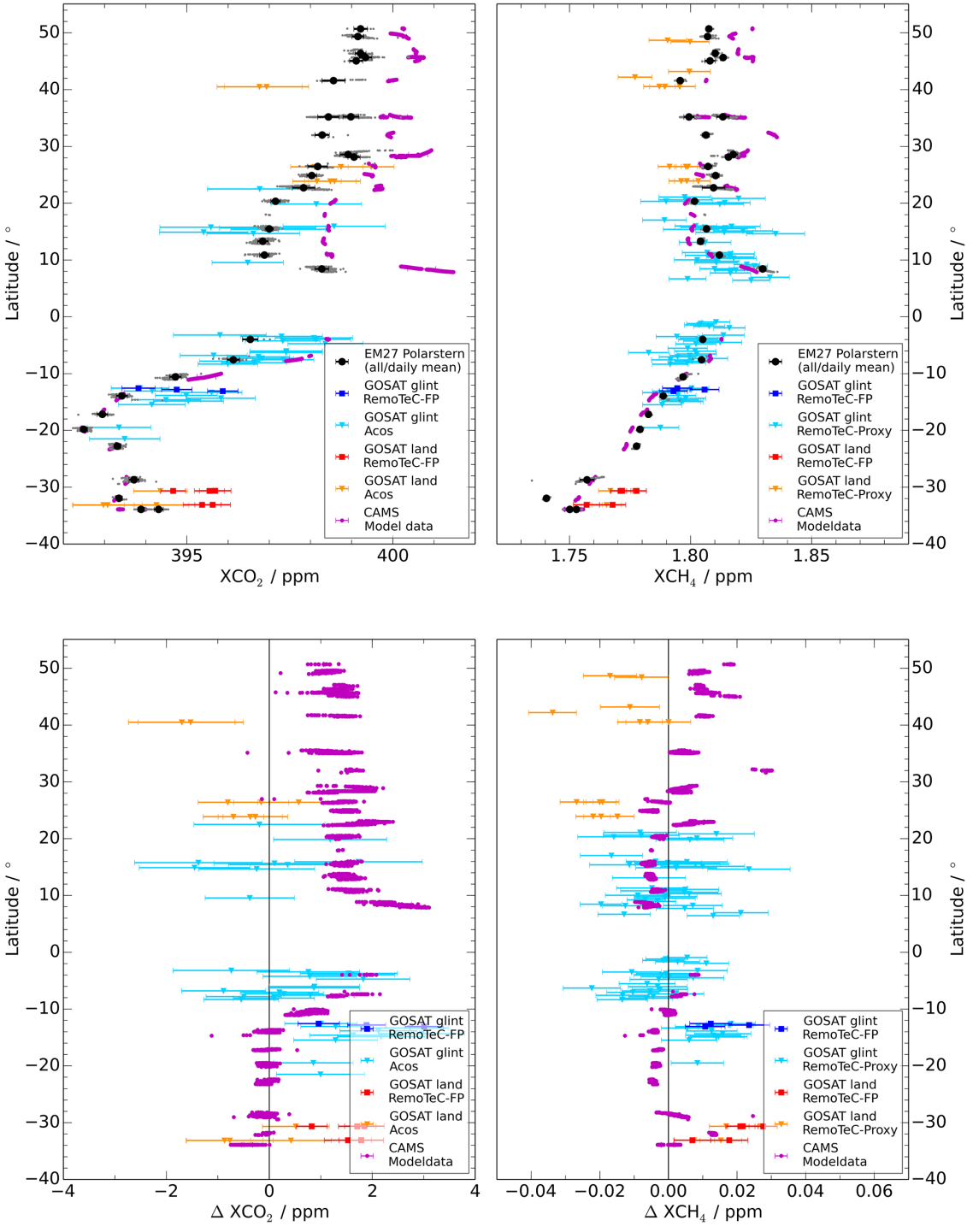

Figure 8. Latitudinal transects of XCO_2 (left) and XCH_4 (right) for the ship-borne EM27/SUN measurements (daily averages: black dots; all data: gray dots) and various correlative data sets (top) as well as differences of the latter to our ship records (bottom). For XCO_2, correlative data sets are the RemoTeC-FP retrievals from GOSAT (ocean glint: blue; land nadir: red), the ACOS retrievals from GOSAT (ocean glint: light blue; land nadir: orange), and XCO_2 modeled by the CAMS model (purple). For XCH_4, correlative data sets are the RemoTeC-FP retrievals from GOSAT (ocean glint: blue; land nadir: red), the RemoTeC-proxy retrievals from GOSAT (ocean glint: light blue; land nadir: orange), and XCH_4 modeled by the CAMS model (purple). For GOSAT, soundings are coincident whenever they are conducted within 5° latitude/longitude of the ship track and within a ±4h time frame. XCO_2 and XCH_4 differences shown in the lower panels are calculated according to $\Delta = X - \langle X_{\mathrm{EM27}} \rangle_{4\,\mathrm{h}}$ where the brackets indicate averaging over 4 h.

exhaust of RV *Polarstern* itself were excluded from the data via the EP filter (see Sect. 3.2).

For XCH_4, Fig. 8 (right), the EM27/SUN soundings find a N–S gradient of roughly 0.06 ppm between ∼ 45° N and ∼ 30° S. Diurnal and day-to-day variability on the order of 0.01 to 0.02 ppm can be observed around 30° S 35° N. Tentatively, latitudinal variability in XCH_4 and XCO_2 follows similar patterns. For example, one might speculate whether XCO_2 and XCH_4 increasing towards the northern tropics (∼ 10° N) are related to emissions of both gases from biomass burning. Though, the inner tropics lack data to confirm that hypothesis.

Both GOSAT XCO_2 retrievals, RemoTeC-FP and ACOS, generally match the EM27/SUN observations within 2 ppm. Due to sparse data coverage, RemoTeC-FP does not allow for assessing the N–S gradient. The ACOS retrievals tentatively show a weaker N–S gradient due to XCO_2 land-nadir soundings north of 23° being somewhat lower than the ship records. Scatter of the data, however, hinders robust conclusions.

The GOSAT RemoTeC-FP and RemoTeC-Proxy XCH_4 retrievals, both agree with the ship-borne records to mostly within 0.02 ppm. As for XCO_2, the yield from RemoTeC-FP is too low to infer robust conclusions but overall RemoTeC-FP delivers XCH_4 offset by 0.01 to 0.02 ppm compared to RemoTeC-Proxy retrievals. The latter fit the validation data particularly well for the tropical ocean-glint soundings. The land-nadir soundings north of 23° N show greater differences of 0.03 to 0.04 ppm, i.e., both RemoTeC-Proxy XCH_4 and ACOS XCO_2, reveal larger differences for the northern mid-latitude land-nadir observations than for the low-latitude ocean-glint soundings. Given that both algorithms and both species are affected, the most likely explanation is that our coincidence criterion is too loose to assume homogeneous concentration fields in the mid-latitudes.

The XCO_2 modeled by CAMS shows an overall excellent agreement to our ship-borne records. In the northern extratropics an offset of 1 to 2 ppm is consistent with an independent evaluation done by Agusti-Panareda et al. (2015, ECMWF Tech. Memo) using TCCON data at several sites in the Northern Hemisphere extratropics. This model bias is linked to errors in the modeled CO_2 fluxes which will be addressed by the CO_2 flux adjustment scheme under development in the CAMS forecasting system. Despite this model bias, the small variations introduced by transport processes can be resolved by both model and measurements. Differences are larger in the tropics where the model overestimates XCO_2. It is clear that the model is not able to represent accurately the CO_2 emissions from West Africa characterized by widespread biomass burning. Due to persistent cloud cover, the ship records lack data in the inner tropics; this hinders further investigation of this source related error. Smaller discrepancies of less than 1 ppm are found in the Southern Hemisphere background air. The smoothing effects introduced by the averaging kernel matrix are directly taken into account due to the use of the model a priories for the spectral retrieval. These effects are larger in the northern extratropics and tropics, but are found to be negligible in the southern extratropics. For XCH_4, model-measurement deviations are below 0.02 ppm for most of the cases. The discrepancies are also larger in the Northern Hemisphere where XCH_4 fluxes are strongest, but the relative differences are much smaller than for XCO_2.

Overall, the deployment of the EM27/SUN spectrometer on RV *Polarstern* demonstrated that the inferred latitudinal transects of XCO_2 and XCH_4 were of adequate quality to validate soundings from satellites such as GOSAT and to evaluate modeled concentration fields such as provided by the CAMS model. The observations collected during our ∼ 5 week campaign are too sparse too allow for a statistically robust ensemble of coincidences with GOSAT, but demonstrated the potential for providing satellite validation over the oceans where other validation opportunities are sparse. Already a few ship cruises, similar to the one discussed here, conducted each year would make a great asset to XCO_2 and XCH_4 remote sensing from satellites in particular for satellites such as OCO-2 providing much denser data coverage than GOSAT. Despite the snapshot-like nature of our observations, the comparison of the ship records to the CAMS model provided hints at model errors in the CO_2 and CH_4 surface fluxes and model deficiencies in the representation of the chemical sink for XCH_4 in tropical regions. Simultaneously comparing measured and modeled XCO_2 and XCH_4 delivers additional confidence in the conclusions since transport related errors are correlated among the two species, thus helping in the model flux/transport error source attribution.

5 Conclusions

We used a portable EM27/SUN FTS to record direct sunlight spectra on board the German research vessel *Polarstern*. The solar tracking device was adapted in hardware and software such that we could record direct-sun absorption spectra regardless of the ship's movements and achieved a tracking precision better than the required 0.05° for 98.7 % of the onboard measurements. This implies that our tracking system can handle angular accelerations up to $6.5° s^{-2}$. To guarantee adequate accuracy of the retrieved XCO_2 and XCH_4 abundances, we defined several quality filters and correction steps. The data were filtered for intensity fluctuations during recording of the interferogram (DC filter), spurious variations in the retrieved O_2 reference (O_2 filter), and XCO_2 retrievals that were contaminated by the ship's local exhaust plume (EP filter). After quality filtering, we corrected for a spurious SZA dependency of the retrieved concentration records, and determined an overall scaling factor with respect to the WMO calibration scale. Thus, the final XCO_2 and XCH_4 concentrations are traceable to WMO standards and show an overall precision of 0.11 ppm for XCO_2 and 0.59 ppb for XCH_4, respectively, as estimated from the scat-

ter of retrieved concentrations after subtracting a polynomial background.

The campaign record of XCO_2 and XCH_4 showed the expected north to south gradient that was overlayed by regional meteorological transport effects. The quality of our ship-based records allowed for comparisons to XCO_2 and XCH_4 retrieved from GOSAT or modeled concentration fields. Although the number of satellite coincidences was low, both the ACOS/GOSAT XCO_2 and RemoTeC-proxy/GOSAT XCH_4 tended to underestimate the interhemispheric gradient due low retrieved concentrations in the northern extra-tropics. The comparison between the CAMS model and the ship records showed excellent agreement for XCH_4 and a systematic high bias for XCO_2 in the Northern Hemisphere associated with CO_2 surface fluxes.

These comparisons recommend our setup, based on the EM27/SUN FTS and a fast solar tracker, to be used for validating models and satellites, e.g., through future deployments on moving platforms such as research vessels, other ships, or land-based vehicles.

The data collected during the RV *Polarstern* cruise is publicly available on the PANGEA archive (PANGEA, 2014) as Supplement to this document or upon request.

Appendix A

Remote sensing instruments are usually not uniformly sensitive to all layers in the atmosphere. The averaging kernel matrix weights the contribution of individual layers to the final retrieved column. The averaging kernel matrix depends on the ILS, solar zenith angle and other parameters. In order to compare the retrieval with other products, one has to include the averaging kernel matrix in the comparison as suggested by (Rodgers et al., 2003) and can be written as follows:

$$c_\mathrm{i} = \boldsymbol{h}^T \boldsymbol{x}_i = \boldsymbol{h}^T \mathbf{A} \boldsymbol{x}_\mathrm{true} + \boldsymbol{h}^T (\mathbf{I} - \mathbf{A}) \boldsymbol{x}_\mathrm{apr} + \epsilon_i . \quad \text{(A1)}$$

Here the retrieved total column c_i from the instrument i is being calculated using the total column operator $\boldsymbol{h}$ and the averaging kernel matrix $\mathbf{A}$ on the state vector $\boldsymbol{x}_i$. $\boldsymbol{x}_\mathrm{true}$ is the true, usually unknown value, ϵ_i any kind of errors and $\mathbf{I}$ represents the unity matrix. A comparison to a high resolution profile (e.g., aircraft profile or model) can be calculated assuming the state vector $\boldsymbol{x}_\mathrm{true}$ being the high resolution profile. In case of $\boldsymbol{x}_\mathrm{true} = \boldsymbol{x}_\mathrm{apr}$, the smoothing effect of the averaging kernel cancels out, and both profiles can be compared directly just by applying the total column operator.

Applying the total column operator $\boldsymbol{h}$ on the averaging kernel matrix $\mathbf{A}$ one gets the total column sensitivity. This can be pictured as the retrieval response to a delta function perturbation in a distinct retrieval layer. Figure A1 shows the retrieval total column sensitivity for the target species CO_2 and CH_4 in dependence on layer pressure (height) and solar zenith angle. Deviations from the ideal value of one can only be found in very high layers or shallow solar zenith angles.

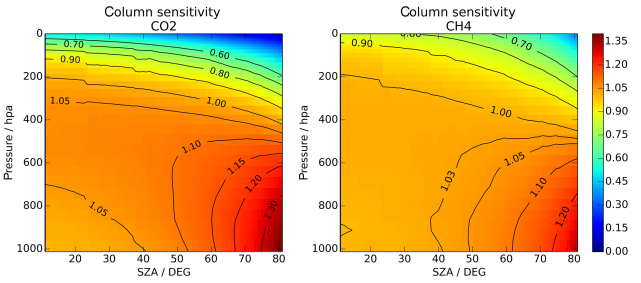

Figure A1. Retrieval total column sensitivity of the target species in dependence of the layer pressure and solar zenith angle (SZA). The data are averaged over three consecutive campaign days (24 March, 31 March and 8 April). The figures can be interpreted as the factor that the total column product will be enhanced, if one additional molecule would be added to a distinct pressure layer.

The Supplement related to this article is available online at doi:10.5194/amt-8-5023-2015-supplement.

Acknowledgements. Friedrich Klappenbach, Marco Bertleff, Julian Kostinek, and André Butz are supported by the Emmy-Noether program of the Deutsche Forschungsgemeinschaft (DFG) through grant BU2599/1-1 (RemoteC). This work is supported by the Copernicus Programme funded by the European Union. We gratefully thank the crew of the RV *Polarstern* for their forthcoming and expert support. We thank Alfred Wegener Institute (AWI), Helmholtz Centre for Polar and Marine Research, for operating RV *Polarstern* and granting access to its infrastructures. We thank Otto Hasekamp and the RemoTeC team at the Netherlands Institute for Space Research (SRON) for co-developing the RemoTeC algorithm and providing RemoTeC/GOSAT retrievals. We thank Christopher O'Dell and the ACOS team at Colorado State University (CSU) and the NASA Jet Propulsion Laboratory for providing ACOS GOSAT retrievals. We thank Matthäus Kiel and Matthias Frey for suggesting the DC quality criteria. Thanks again to Matthäus Kiel for providing the initial version of "Calpy".

The article processing charges for this open-access publication were covered by a Research Centre of the Helmholtz Association.

Edited by: D. Feist

References

Agustí-Panareda, A., Massart, S., Chevallier, F., Boussetta, S., Balsamo, G., Beljaars, A., Ciais, P., Deutscher, N. M., Engelen, R., Jones, L., Kivi, R., Paris, J.-D., Peuch, V.-H., Sherlock, V., Vermeulen, A. T., Wennberg, P. O., and Wunch, D.: Forecasting global atmospheric CO_2, Atmos. Chem. Phys., 14, 11959–11983, doi:10.5194/acp-14-11959-2014, 2014.

Bergamaschi, P., Frankenberg, C., Meirink, J. F., Krol, M., Villani, M. G., Houweling, S., Dentener, F., Dlugokencky, E. J., Miller, J. B., Gatti, L. V., Engel, A., and Levin, I.: Inverse modeling of global and regional CH_4 emissions using SCIAMACHY satellite retrievals, J. Geophys. Res.-Atmos., 114, D22301, doi:10.1029/2009JD012287, 2009.

Boussetta, S., Balsamo, G., Beljaars, A., Agusti-Panareda, A., Calvet, J.-C., Jacobs, C., van den Hurk, B., Viterbo, P., Lafont, S., Dutra, E., Jarlan, L., Balzarolo, M., Papale, D., and van der Werf, G.: Natural carbon dioxide exchanges in the ECMWF integrated forecasting system: implementation and offline validation, J. Geophys Res.-Atmos., 118, 1–24, doi:10.1002/jgrd.50488, 2013.

Bovensmann, H., Burrows, J., Buchwitz, M., Frerick, J., Noël, S., Rozanov, V., Chance, K., and Goede, A.: SCIAMACHY: mission objectives and measurement modes, J. Atmos. Sci., 56, 127–150, 1999.

Bovensmann, H., Buchwitz, M., Burrows, J. P., Reuter, M., Krings, T., Gerilowski, K., Schneising, O., Heymann, J., Tretner, A., and Erzinger, J.: A remote sensing technique for global monitoring of power plant CO_2 emissions from space and related applications, Atmos. Meas. Tech., 3, 781–811, doi:10.5194/amt-3-781-2010, 2010.

Burrows, J., Hölzle, E., Goede, A., Visser, H., and Fricke, W.: SCIAMACHY scanning imaging absorption spectrometer for atmospheric chartography, earth Observation, Acta Astronaut., 35, 445–451, doi:10.1016/0094-5765(94)00278-T, 1995.

Butz, A., Guerlet, S., Hasekamp, O., Schepers, D., Galli, A., Aben, I., Frankenberg, C., Hartmann, J.-M., Tran, H., Kuze, A., Keppel-Aleks, G., Toon, G., Wunch, D., Wennberg, P., Deutscher, N., Griffith, D., Macatangay, R., Messerschmidt, J., Notholt, J., and Warneke, T.: Toward accurate CO_2 and CH_4 observations from GOSAT, Geophys. Res. Lett., 38, L14812, doi:10.1029/2011GL047888, 2011.

Butz, A., Guerlet, S., Hasekamp, O. P., Kuze, A., and Suto, H.: Using ocean-glint scattered sunlight as a diagnostic tool for satellite remote sensing of greenhouse gases, Atmos. Meas. Tech., 6, 2509–2520, doi:10.5194/amt-6-2509-2013, 2013.

Chevallier, F., Bréon, F.-M., and Rayner, P. J.: Contribution of the Orbiting Carbon Observatory to the estimation of CO_2 sources and sinks: theoretical study in a variational data assimilation framework, J. Geophys. Res.-Atmos., 112, D09307, doi:10.1029/2006JD007375, 2007.

Chevallier, F., Ciais, P., Conway, T. J., Aalto, T., Anderson, B. E., Bousquet, P., Brunke, E. G., Ciattaglia, L., Esaki, Y., Fröhlich, M., Gomez, A., Gomez-Pelaez, A. J., Haszpra, L., Krummel, P. B., Langenfelds, R. L., Leuenberger, M., Machida, T., Maignan, F., Matsueda, H., Morguí, J. A., Mukai, H., Nakazawa, T., Peylin, P., Ramonet, M., Rivier, L., Sawa, Y., Schmidt, M., Steele, L. P., Vay, S. A., Vermeulen, A. T., Wofsy, S., and Worthy, D.: CO_2 surface fluxes at grid point scale estimated from a global 21 year reanalysis of atmospheric measurements, J. Geophys. Res.-Atmos., 115, D21307, doi:10.1029/2010JD013887, 2010.

Crisp, D., Fisher, B. M., O'Dell, C., Frankenberg, C., Basilio, R., Bösch, H., Brown, L. R., Castano, R., Connor, B., Deutscher, N. M., Eldering, A., Griffith, D., Gunson, M., Kuze, A., Mandrake, L., McDuffie, J., Messerschmidt, J., Miller, C. E., Morino, I., Natraj, V., Notholt, J., O'Brien, D. M., Oyafuso, F., Polonsky, I., Robinson, J., Salawitch, R., Sherlock, V., Smyth, M., Suto, H., Taylor, T. E., Thompson, D. R., Wennberg, P. O., Wunch, D., and Yung, Y. L.: The ACOS CO_2 retrieval algorithm – Part II: Global X_{CO2} data characterization, Atmos. Meas. Tech., 5, 687–707, doi:10.5194/amt-5-687-2012, 2012.

Denning, A. S., Fung, I. Y., and Randall, D.: Latitudinal gradient of atmospheric CO_2 due to seasonal exchange with land biota, Nature, 376, 240–243, 1995.

Deutscher, N. M., Griffith, D. W. T., Bryant, G. W., Wennberg, P. O., Toon, G. C., Washenfelder, R. A., Keppel-Aleks, G., Wunch, D., Yavin, Y., Allen, N. T., Blavier, J.-F., Jiménez, R., Daube, B. C., Bright, A. V., Matross, D. M., Wofsy, S. C., and Park, S.: Total column CO_2 measurements at Darwin, Australia – site description and calibration against in situ aircraft profiles, Atmos. Meas. Tech., 3, 947–958, doi:10.5194/amt-3-947-2010, 2010. 2010.

Dohe, S., Sherlock, V., Hase, F., Gisi, M., Robinson, J., Sepúlveda, E., Schneider, M., and Blumenstock, T.: A method to correct sampling ghosts in historic near-infrared Fourier transform spectrometer (FTS) measurements, Atmos. Meas. Tech., 6, 1981–1992, doi:10.5194/amt-6-1981-2013, 2013.

Fleming, E. L., Chandra, S., Schoeberl, M. R., and Barnett, J. J.: Monthly mean global climatology of temperature, wind, geopotential height, and pressure for 0–120 km, Adv. Space Res., 10, 3–12, doi:10.1016/0273-1177(90)90230-W, 1988.

Frey, M., Hase, F., Blumenstock, T., Groß, J., Kiel, M., Mengistu Tsidu, G., Schäfer, K., Sha, M. K., and Orphal, J.: Calibration and instrumental line shape characterization of a set of portable FTIR spectrometers for detecting greenhouse gas emissions, Atmos. Meas. Tech., 8, 3047–3057, doi:10.5194/amt-8-3047-2015, 2015.

García, O. E., Schneider, M., Redondas, A., González, Y., Hase, F., Blumenstock, T., and Sepúlveda, E.: Investigating the long-term evolution of subtropical ozone profiles applying ground-based FTIR spectrometry, Atmos. Meas. Tech., 5, 2917–2931, doi:10.5194/amt-5-2917-2012, 2012.

Geibel, M. C., Gerbig, C., and Feist, D. G.: A new fully automated FTIR system for total column measurements of greenhouse gases, Atmos. Meas. Tech., 3, 1363–1375, doi:10.5194/amt-3-1363-2010, 2010.

Gisi, M., Hase, F., Dohe, S., and Blumenstock, T.: Camtracker: a new camera controlled high precision solar tracker system for FTIR-spectrometers, Atmos. Meas. Tech., 4, 47–54, doi:10.5194/amt-4-47-2011, 2011.

Gisi, M., Hase, F., Dohe, S., Blumenstock, T., Simon, A., and Keens, A.: XCO_2-measurements with a tabletop FTS using solar absorption spectroscopy, Atmos. Meas. Tech., 5, 2969–2980, doi:10.5194/amt-5-2969-2012, 2012.

Guerlet, S., Butz, A., Schepers, D., Basu, S., Hasekamp, O. P., Kuze, A., Yokota, T., Blavier, J.-F., Deutscher, N. M., Griffith, D. W., Hase, F., Kyro, E., Morino, I., Sherlock, V., Sussmann, R., Galli, A., and Aben, I.: Impact of aerosol and thin cirrus on retrieving and validating XCO_2 from GOSAT shortwave infrared measurements, J. Geophys. Res.-Atmos., 118, 4887–4905, doi:10.1002/jgrd.50332, 2013.

Hase, F., Blumenstock, T., and Paton-Walsh, C.: Analysis of the instrumental line shape of high-resolution Fourier transform IR spectrometers with gas cell measurements and new retrieval software, Appl. Optics, 38, 3417–3422, doi:10.1364/AO.38.003417, 1999.

Hase, F., Hannigan, J., Coffey, M., Goldman, A., Höpfner, M., Jones, N., Rinsland, C., and Wood, S.: Intercomparison of retrieval codes used for the analysis of high-resolution, ground-based FTIR measurements, J. Quant. Spectrosc. Ra., 87, 25–52, doi:10.1016/j.jqsrt.2003.12.008, 2004.

Hase, F., Blumenstock, T., Dohe, S., Groß, J., and Kiel, M.: TCCON data from Karlsruhe, Germany, Release GGG2014R1, TCCON data archive, hosted by the Carbon Dioxide Information Analysis Center, Oak Ridge National Laboratory, Oak Ridge, Tennessee, USA, available at: doi:10.14291/tccon.ggg2014.karlsruhe01.R1/1182416, last access: 27 November 2015.

Kalnay, E., Kanamitsu, M., Kistler, R., Collins, W., Deaven, D., Gandin, L., Iredell, M., Saha, S., White, G., Woollen, J., Zhu, Y., Leetmaa, A., Reynolds, R., Chelliah, M., Ebisuzaki, W., Higgins, W., Janowiak, J., Mo, K. C., Ropelewski, C., Wang, J., Jenne, R., and Joseph, D.: The NCEP/NCAR 40-year reanalysis project, B. Am. Meteorol. Soc., 77, 737–471, doi:10.1175/1520-0477(1996)077<0437:TNYRP>2.0.CO;2, 1996.

Kawasaki, M., Yoshioka, H., Jones, N. B., Macatangay, R., Griffith, D. W. T., Kawakami, S., Ohyama, H., Tanaka, T., Morino, I., Uchino, O., and Ibuki, T.: Usability of optical spectrum analyzer in measuring atmospheric CO_2 and CH_4 column densities: inspection with FTS and aircraft profiles in situ, Atmos. Meas. Tech., 5, 2593–2600, doi:10.5194/amt-5-2593-2012, 2012.

Keppel-Aleks, G., Toon, G. C., Wennberg, P. O., and Deutscher, N. M.: Reducing the impact of source brightness fluctuations on spectra obtained by Fourier-transform spectrometry, Appl. Optics, 46, 4774–4779, doi:10.1364/AO.46.004774, 2007a.

Keppel-Aleks, G., Toon, G. C., Wennberg, P. O., and Deutscher, N. M.: Reducing the impact of source brightness fluctuations on spectra obtained by Fourier-transform spectrometry, Appl. Optics, 46, 4774–4779, doi:10.1364/AO.46.004774, 2007b.

Kobayashi, N., Inoue, G., Kawasaki, M., Yoshioka, H., Minomura, M., Murata, I., Nagahama, T., Matsumi, Y., Tanaka, T., Morino, I., and Ibuki, T.: Remotely operable compact instruments for measuring atmospheric CO_2 and CH_4 column densities at surface monitoring sites, Atmos. Meas. Tech., 3, 1103–1112, doi:10.5194/amt-3-1103-2010, 2010.

König-Langlo, G.: Radiosonde During POLARSTERN Cruise PS83 (ANT-XXIX/10), Bremerhaven, Germany, available at: doi:10.1594/PANGAEA.832783 (last access: 27 November 2015.), 2014.

Krings, T., Gerilowski, K., Buchwitz, M., Reuter, M., Tretner, A., Erzinger, J., Heinze, D., Pflüger, U., Burrows, J. P., and Bovensmann, H.: MAMAP – a new spectrometer system for column-averaged methane and carbon dioxide observations from aircraft: retrieval algorithm and first inversions for point source emission rates, Atmos. Meas. Tech., 4, 1735–1758, doi:10.5194/amt-4-1735-2011, 2011.

Lamouroux, J., Tran, H., Laraia, A., Gamache, R., Rothman, L., Gordon, I., and Hartmann, J.-M.: Updated database plus software for line-mixing in CO_2 infrared spectra and their test using laboratory spectra in the 1.5–2.3 μm region, XVIth Symposium on High Resolution Molecular Spectroscopy (HighRus-2009) XVIth Symposium on High Resolution Molecular Spectroscopy, J. Quant. Spectrosc. Ra., 111, 2321–2331, doi:10.1016/j.jqsrt.2010.03.006, 2010.

Masarie, K. A., Peters, W., Jacobson, A. R., and Tans, P. P.: ObsPack: a framework for the preparation, delivery, and attribution of atmospheric greenhouse gas measurements, Earth Syst. Sci. Data, 6, 375–384, doi:10.5194/essd-6-375-2014, 2014.

Massart, S., Agusti-Panareda, A., Aben, I., Butz, A., Chevallier, F., Crevoisier, C., Engelen, R., Frankenberg, C., and Hasekamp, O.: Assimilation of atmospheric methane products into the MACC-II system: from SCIAMACHY to TANSO and IASI, Atmos. Chem. Phys., 14, 6139–6158, doi:10.5194/acp-14-6139-2014, 2014.

Meirink, J. F., Eskes, H. J., and Goede, A. P. H.: Sensitivity analysis of methane emissions derived from SCIAMACHY observations through inverse modelling, Atmos. Chem. Phys., 6, 1275–1292, doi:10.5194/acp-6-1275-2006, 2006.

Messerschmidt, J., Machatangay, R., Notholt, J., Petri, C., Warneke, T., and Weinzierl, C.: Side by side measurements of CO_2 by ground-based Fourier transform spectrometry (FTS), Tellus B, 62, 749–758, doi:10.1111/j.1600-0889.2010.00491.x, 2010.

Notholt, J., Beninga, I., and Schrems, O.: Shipborne FT-IR Measurements of Atmospheric Trace Gases on a South (33° S) to North (53° N) Atlantic Traverse, Appl. Spectrosc., 49, 1525–1527, 1995.

O'Dell, C. W., Connor, B., Bösch, H., O'Brien, D., Frankenberg, C., Castano, R., Christi, M., Eldering, D., Fisher, B., Gunson, M., McDuffie, J., Miller, C. E., Natraj, V., Oyafuso, F., Polonsky, I., Smyth, M., Taylor, T., Toon, G. C., Wennberg, P. O., and Wunch, D.: The ACOS CO_2 retrieval algorithm – Part 1: Description and validation against synthetic observations, Atmos. Meas. Tech., 5, 99–121, doi:10.5194/amt-5-99-2012, 2012.

PANGEA: XCO_2 and XCH_4 Total Column Measurement ANT XXIX/10 North–South Gradient, PANGEA, Bremerhaven, Germany, available at: doi:10.1594/PANGAEA.843880 (last access: 27 November 2015.), 2014.

Peters, W., Jacobson, A. R., Sweeney, C., Andrews, A. E., Conway, T. J., Masarie, K., Miller, J. B., Bruhwiler, L. M. P., Pétron, G., Hirsch, A. I., Worthy, D. E. J., van der Werf, G. R., Randerson, J. T., Wennberg, P. O., Krol, M. C., and Tans, P. P.: An atmospheric perspective on North American carbon dioxide exchange: CarbonTracker, P. Natl. Acad. Sci. USA, 104, 18925–18930, doi:10.1073/pnas.0708986104, 2007.

Petri, C., Warneke, T., Jones, N., Ridder, T., Messerschmidt, J., Weinzierl, T., Geibel, M., and Notholt, J.: Remote sensing of CO_2 and CH_4 using solar absorption spectrometry with a low resolution spectrometer, Atmos. Meas. Tech., 5, 1627–1635, doi:10.5194/amt-5-1627-2012, 2012.

Peylin, P., Law, R. M., Gurney, K. R., Chevallier, F., Jacobson, A. R., Maki, T., Niwa, Y., Patra, P. K., Peters, W., Rayner, P. J., Rödenbeck, C., van der Laan-Luijkx, I. T., and Zhang, X.: Global atmospheric carbon budget: results from an ensemble of atmospheric CO_2 inversions, Biogeosciences, 10, 6699–6720, doi:10.5194/bg-10-6699-2013, 2013.

Rodgers, C. D. and Connor, B. J.:Intercomparison of remote sounding instruments, J. Geophys. Res.-Atmos., 108, 2156–2202, doi:10.1029/2002JD002299, 2003.

Rayner, P. J. and O'Brien, D. M.: The utility of remotely sensed CO_2 concentration data in surface source inversions, Geophys. Res. Lett., 28, 175–178, doi:10.1029/2000GL011912, 2001.

Rothman, L., Gordon, I., Barbe, A., Benner, D., Bernath, P., Birk, M., Boudon, V., Brown, L., Campargue, A., Champion, J.-P., Chance, K., Coudert, L., Dana, V., Devi, V., Fally, S., Flaud, J.-M., Gamache, R., Goldman, A., Jacquemart, D., Kleiner, I., Lacome, N., Lafferty, W., Mandin, J.-Y., Massie, S., Mikhailenko, S., Miller, C., Moazzen-Ahmadi, N., Naumenko, O., Nikitin, A., Orphal, J., Perevalov, V., Perrin, A., Predoi-Cross, A., Rinsland, C., Rotger, M., Ŝimeĉková, M., Smith, M., Sung, K., Tashkun, S., Tennyson, J., Toth, R., Vandaele, A., and Auwera, J. V.: The HITRAN 2008 molecular spectroscopic database, J. Quant. Spectrosc. Ra., 110, 533–572, doi:10.1016/j.jqsrt.2009.02.013, 2009.

Schepers, D., Guerlet, S., Butz, A., Landgraf, J., Frankenberg, C., Hasekamp, O., Blavier, J.-F., Deutscher, N. M., Griffith, D. W. T., Hase, F., Kyro, E., Morino, I., Sherlock, V., Sussmann, R., and Aben, I.: Methane retrievals from Greenhouse Gases Observing Satellite (GOSAT) shortwave infrared measurements: performance comparison of proxy and physics retrieval algorithms, J. Geophys. Res.-Atmos., 117, D10307, doi:10.1029/2012JD017549, 2012.

Schneider, M., Cuevas, E., Hernández, E. S., Hase, F., Blumenstock, T., García, J. C. G., and Ángel J. Gómez Peláez: Total Carbon Column Observing Network (TCCON) activities at Izaña, Tenerife, Optica pura y aplicada, 1–4, available at: http://dialnet.unirioja.es/servlet/articulo?codigo=3867004 (last access: 17 July 2015), 2012.

Schoeberl, M. R., Newman, P. A., and Lait, L. R.: Gridded meeorological data (analysis) from NMC:GG1X1:E01:SSIAVN, available at: http://acdb-ext.gsfc.nasa.gov/Data_services/automailer/ (last access: 17 July 2015), 2014.

Stocker, T. F., Dahe, Q., and Plattner, G.-K.: Climate Change 2013: The Physical Science Basis, Working Group I Contribution to the Fifth Assessment Report of the Intergovernmental Panel on Climate Change, Summary for Policymakers (IPCC, 2013), Cambridge University Press, Cambridge, UK and New York, NY, USA, p. 54, 2013.

TCCON-Wiki: TCCON-Wiki, available at: https://tccon-wiki.caltech.edu/, last access: 17 July 2015.

Warneke, T., de Beek, R., Buchwitz, M., Notholt, J., Schulz, A., Velazco, V., and Schrems, O.: Shipborne solar absorption measurements of CO_2, CH_4, N_2O and CO and comparison with SCIAMACHY WFM-DOAS retrievals, Atmos. Chem. Phys., 5, 2029–2034, doi:10.5194/acp-5-2029-2005, 2005.

Wunch, D., Toon, G. C., Wennberg, P. O., Wofsy, S. C., Stephens, B. B., Fischer, M. L., Uchino, O., Abshire, J. B., Bernath, P., Biraud, S. C., Blavier, J.-F. L., Boone, C., Bowman, K. P., Browell, E. V., Campos, T., Connor, B. J., Daube, B. C., Deutscher, N. M., Diao, M., Elkins, J. W., Gerbig, C., Gottlieb, E., Griffith, D. W. T., Hurst, D. F., Jiménez, R., Keppel-Aleks, G., Kort, E. A., Macatangay, R., Machida, T., Matsueda, H., Moore, F., Morino, I., Park, S., Robinson, J., Roehl, C. M., Sawa, Y., Sherlock, V., Sweeney, C., Tanaka, T., and Zondlo, M. A.: Calibration of the Total Carbon Column Observing Network using aircraft profile data, Atmos. Meas. Tech., 3, 1351–1362, doi:10.5194/amt-3-1351-2010, 2010.

Wunch, D., Toon, G., Blavier, J., Waschenfelder, R., Notholt, J., Connor, B., Griffith, D., and SherlockSherlock, V.: The Total Carbon Column Observing Network, Philos. T. Roy. Soc. A, 369, 2087–2112, 2011, doi:10.1098/rsta.2010.0240, 2011.

Wunch, D., Toon, G. C.,Sherlock V., Deutscher N. M., Liu X., Feist, D. G. and Wennberg, P. O.: The Total Carbon Column Observing Network's GGG2014 Data Version. Carbon Dioxide Information Analysis Center, Oak Ridge National Laboratory, Oak Ridge, Tennessee, USA, available at: doi:10.14291/tccon.ggg2014.documentation.R0/1221662, last access: 27 November 2015.